Supporting Information for

Bottom-up assembly of bimetallic nanocluster catalysts from oxide-supported single-atom precursors

Bidyut B. Sarma,[a] Giovanni Agostini,[b] Marcos G. Farpón,[c] Carlo Marini,[b] Norbert Pfänder,[d] Gonzalo Prieto [a,c,*]

[a] Max-Planck-Institut für Kohlenforschung, Kaiser-Wilhelm-Platz 1, 45470 Mülheim an der Ruhr, Germany.

[b] ALBA Synchrotron Light Source, Carrer de la Llum 2-26, 08290, Cerdanyola del Vallès, Barcelona, Spain.

[c] ITQ Instituto de Tecnología Química, Universitat Politècnica de València-Consejo Superior de Investigaciones Científicas (UPV-CSIC), Av. Los Naranjos s/n, 46022 Valencia, Spain.

[d] Max-Planck-Institut für chemische Energiekonversion, Stiftstraße 34-36, 45470 Mülheim an der Ruhr, Germany.

Table of contents

1. Supplementary Figures

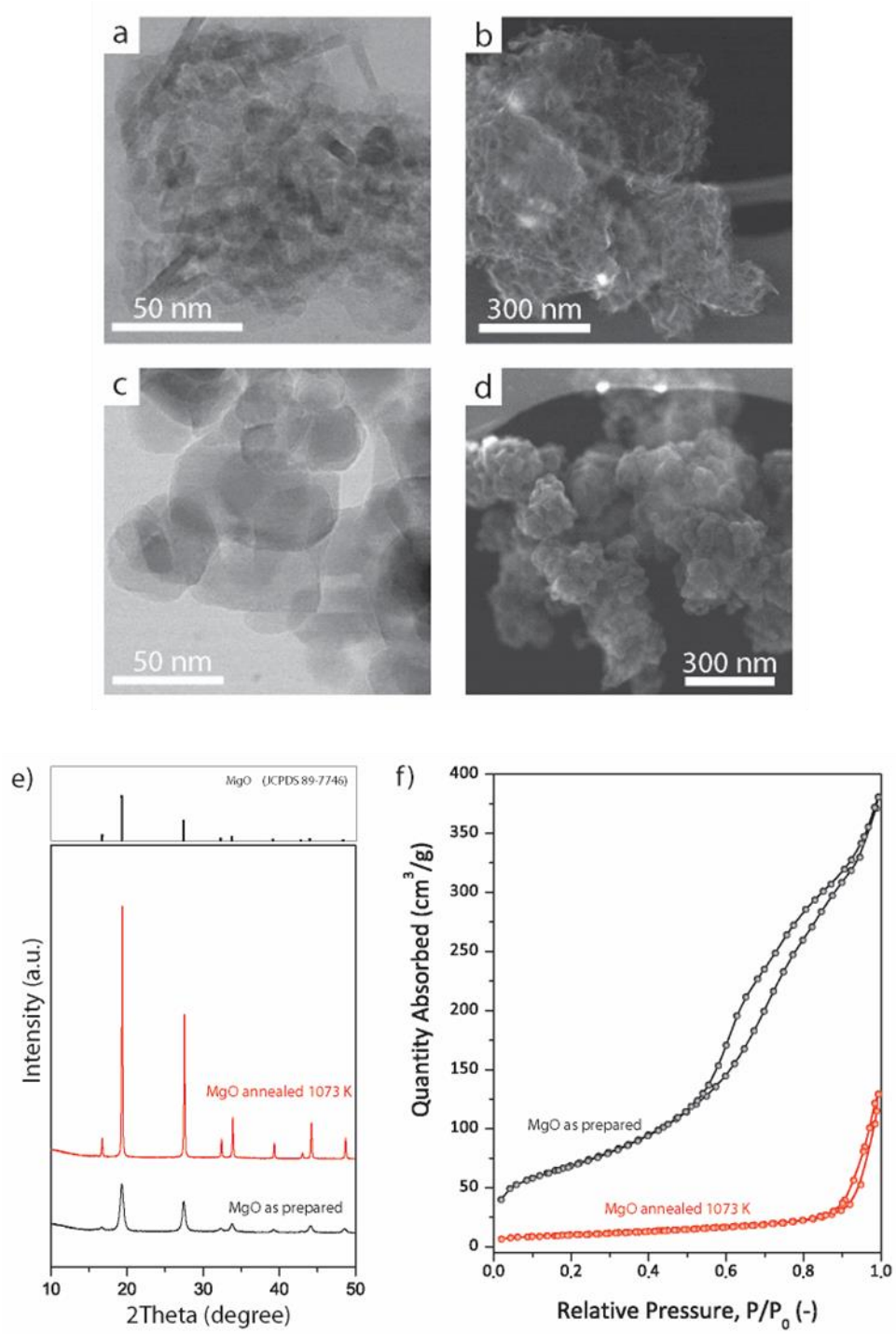

Figure S1: a,c) Bright-field STEM micrographs and b,d) high-resolution SEM micrographs of the MgO support material as-synthesized (a,b) and after annealing in stagnant air at 1073 K (c,d). e) X-ray diffraction patterns and f) N_2-physisorption isotherms for the MgO support material as-synthesized and after annealing in stagnant air at 1073 K, respectively.

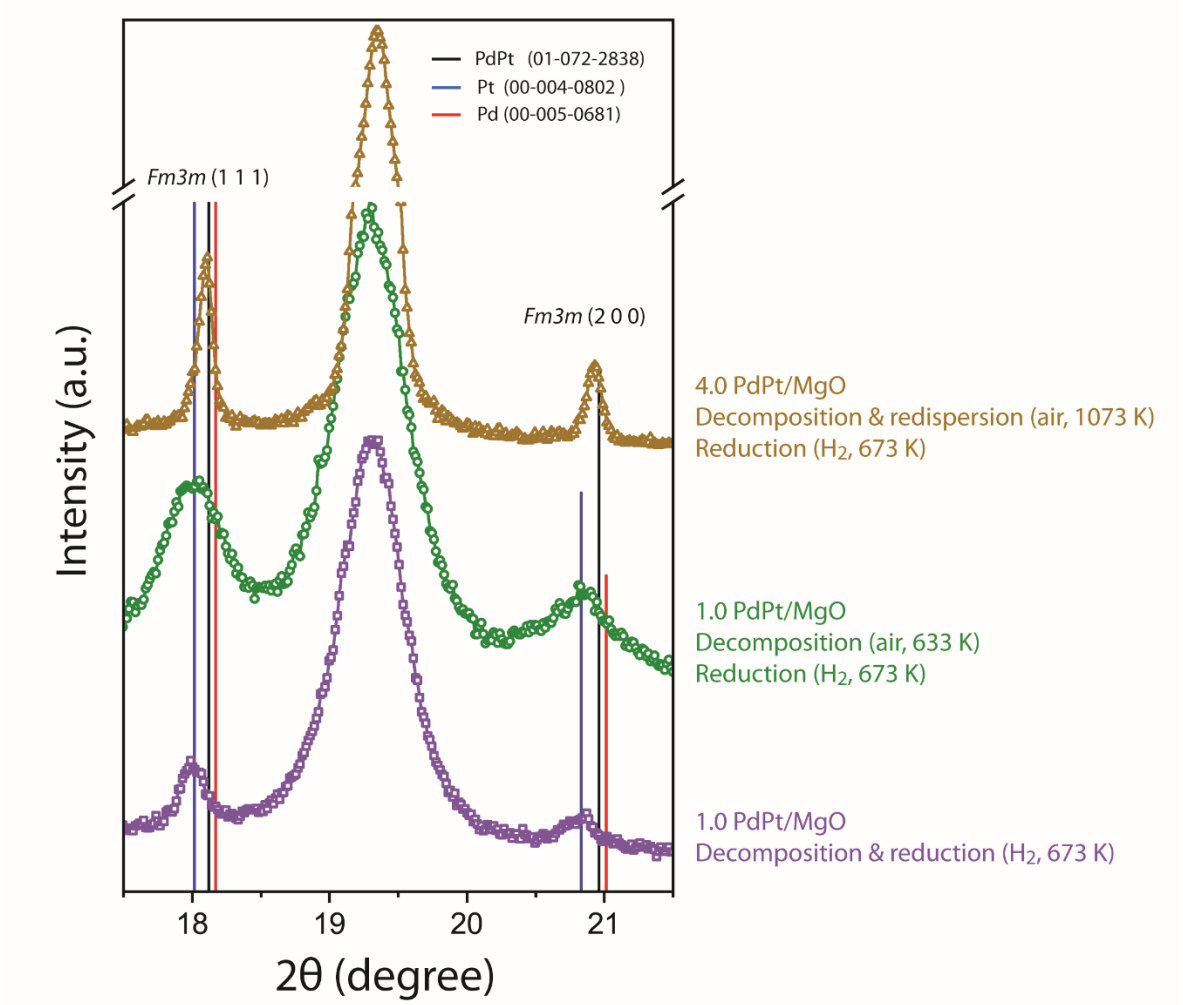

Figure S2: Close-up detail of X-ray diffractions corresponding to the (1 1 1) and (2 0 0) crystallographic planes of cubic *Fm3m* metal nanocrystals in selected PdPt/MgO materials (Pd:Pt=1) synthesized with different surface-specific metal contents and through different activation procedures from metal acetylacetonate precursors. For reference, diffraction lines corresponding to pure Pt and Pd metals, as well as an equimolar PdPt alloy (ICCD PDF-2 database) are also included.

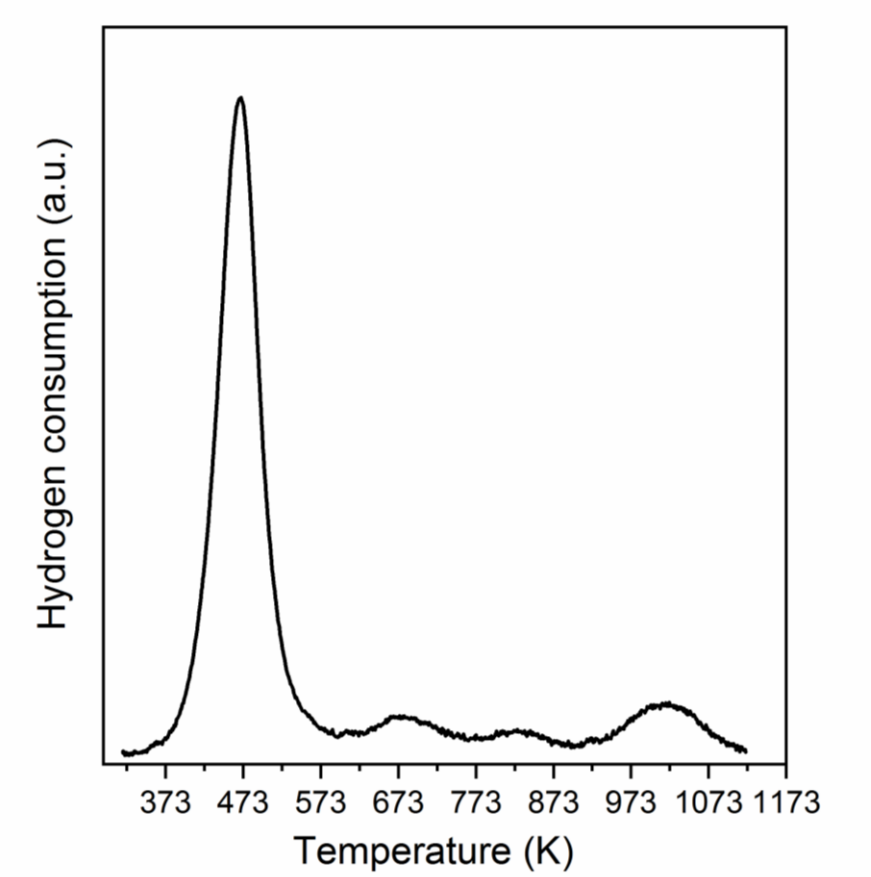

Figure S3: Temperature-programmed reduction profile for a 1.0PdPt/MgO catalyst (Pd:Pt=1) synthesized by decomposition of the metal acetylacetonate precursors in air, followed by metal redispersion in air at 1073 K.

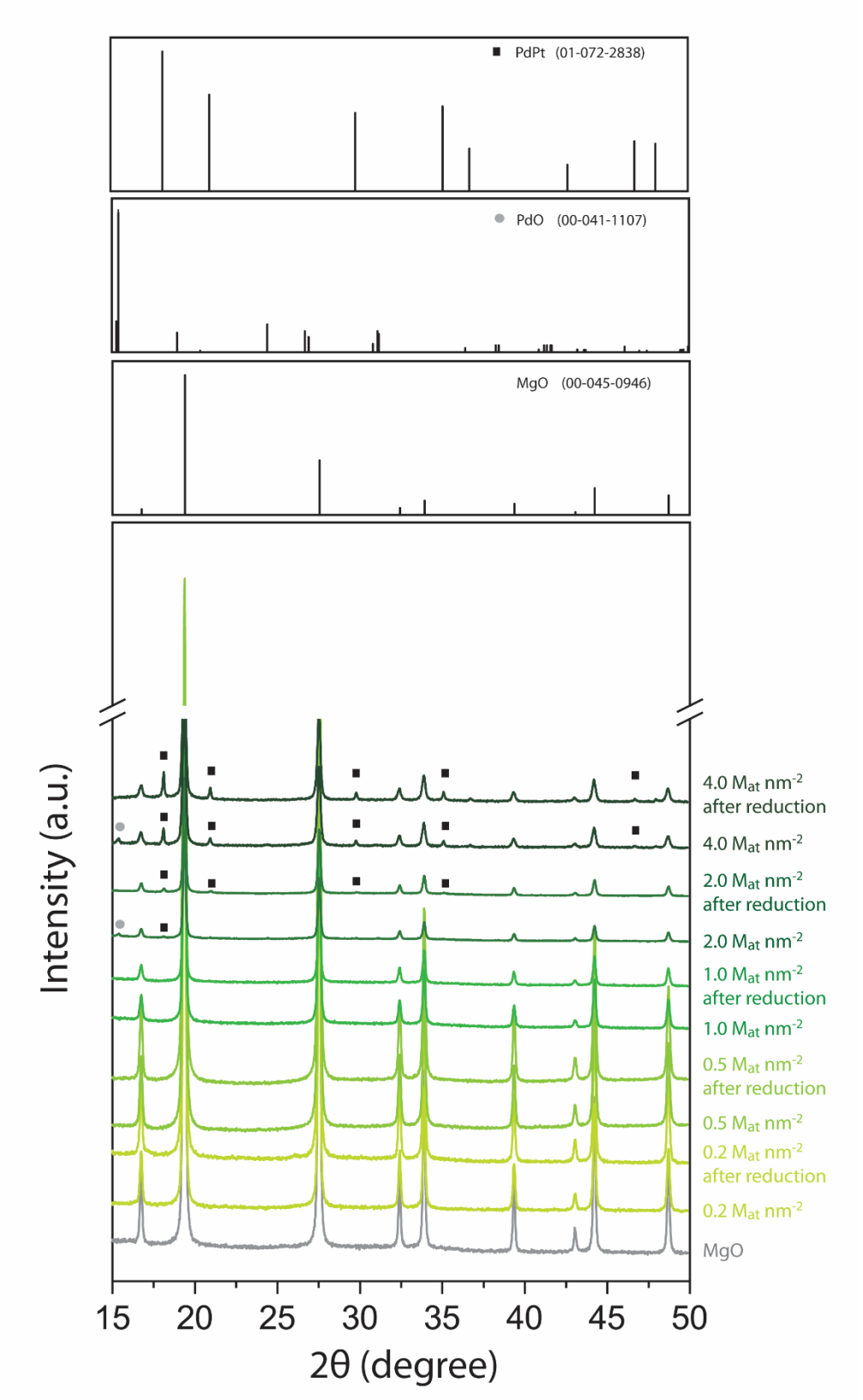

Figure S4: X-ray diffraction patterns for PdPt/MgO materials synthesized with different surface-specific metal contents by decomposition of the metal precursors in air, followed by metal redispersion in air at 1073 K and H_2-reduction at 673 K. Selected diffraction patterns from the ICCD PDF-2 database are also included for reference.

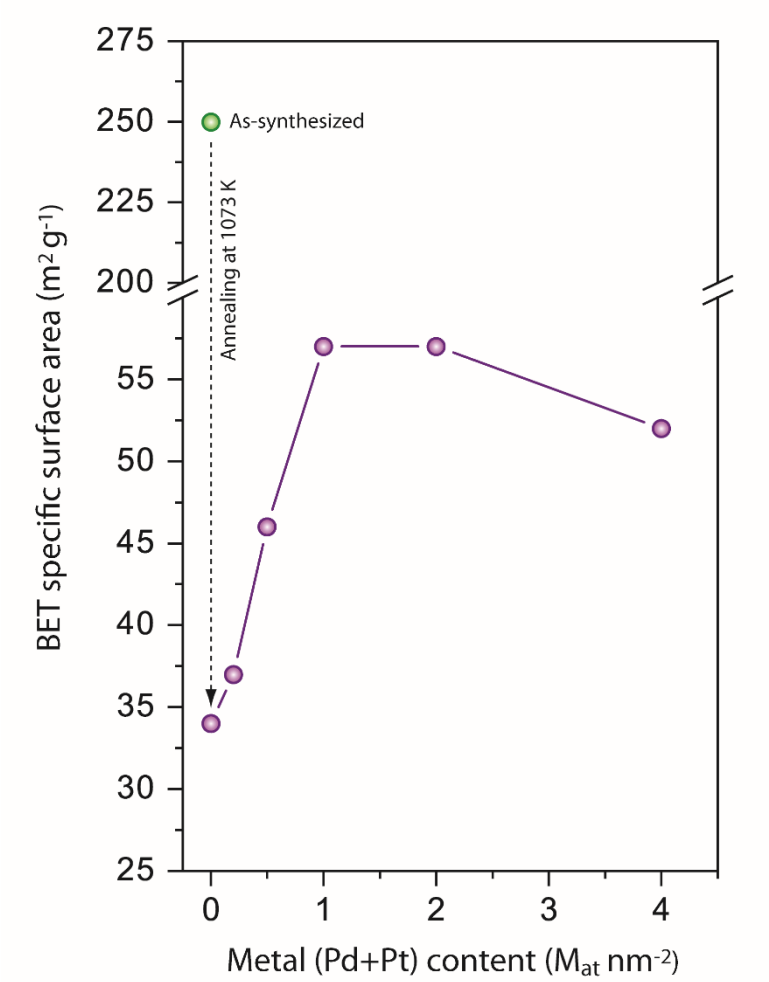

Figure S5: Evolution of the BET specific surface area with the surface-specific metal content for the series of bimetallic PdPt/MgO catalysts subjected to oxidative metal redispersion at 1073 K. As a reference, the specific surface area for the as-synthesized (unannealed) MgO support is also included in the plot.

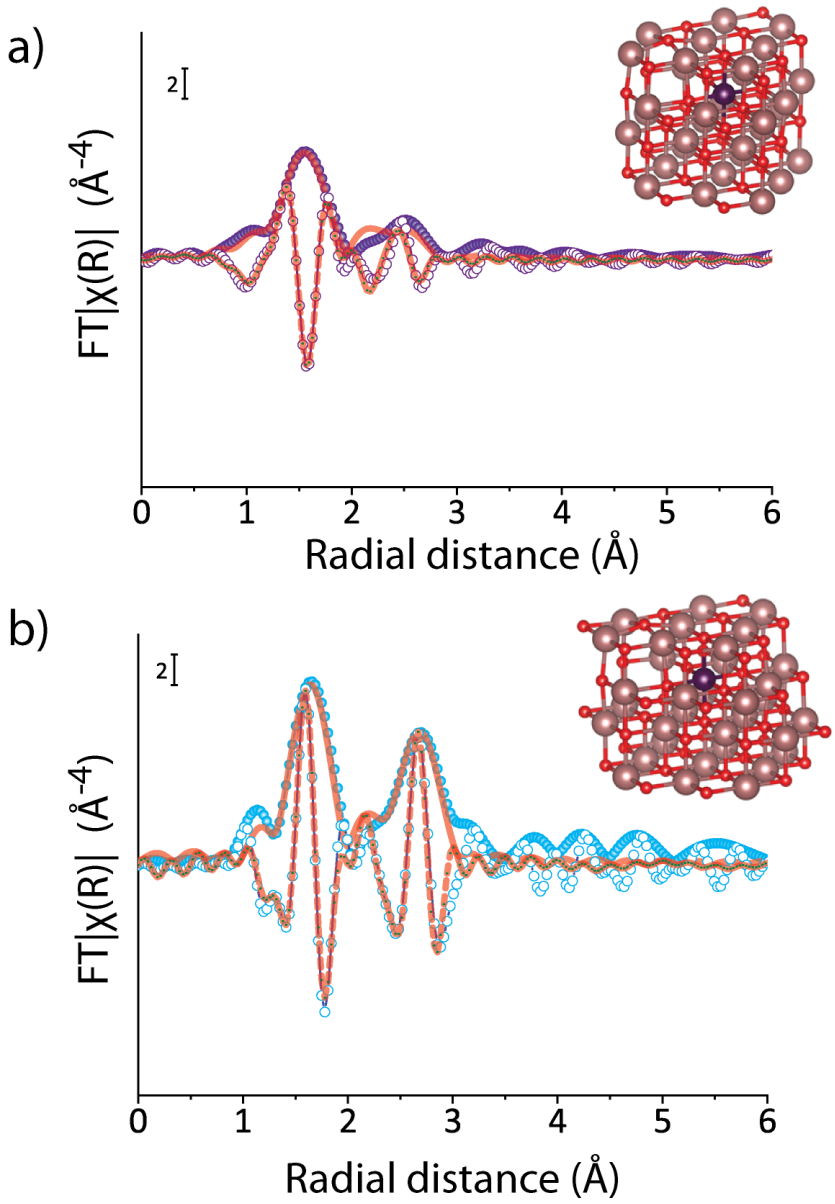

Figure S6: Fourier-transform of the phase-uncorrected k^3-weighted EXAFS function for spectra recorded at the Pd-K (a) and Pt-L_3 (b) XAS edges for 1.0PdPt/MgO synthesized via air calcination followed by oxidative metal redispersion at 1073 K. Scatter traces correspond to experimental data (closed symbols: real components; open symbols: imaginary components). Full lines correspond to the fits of the experimental data to structural models corresponding to single M^{4+} cations (M=Pt, Pd) substituting a Mg^{2+} cation in a regular subsurface lattice position and stabilized by a neighboring V''_{Mg} vacancy, as depicted in the 3D ball-bar models. Color codes in the structure models: red: O, purple: Mg, navy: Pd or Pt, respectively.

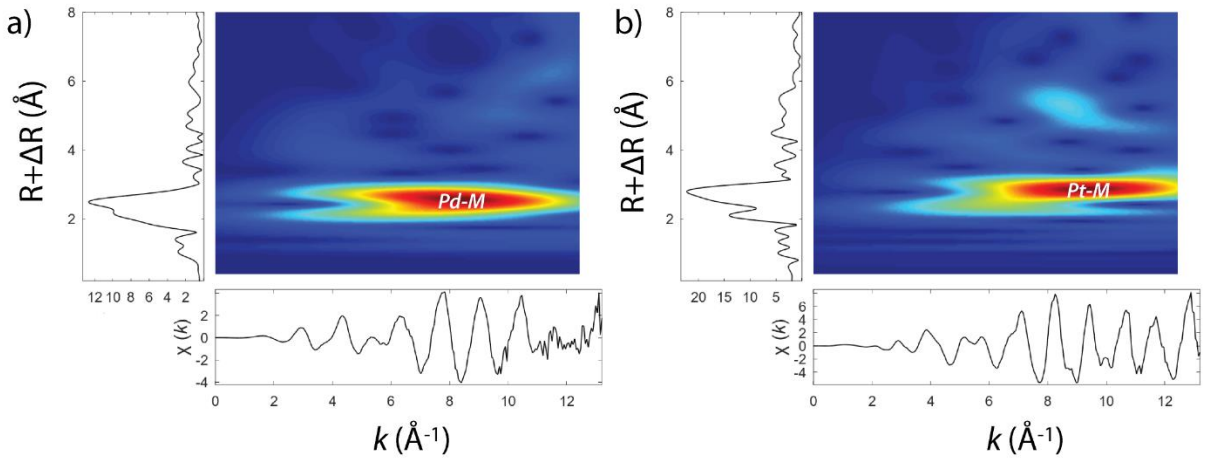

Figure S7: Wavelet transform of the EXAFS function at the Pd-K (a) and Pt-L_3 (b) absorption edges for a 1.0PdPt/MgO catalyst synthesized via air calcination at 623 K followed by *in situ* reduction in 20%H_2/N_2 in the XAS cell. M stands for either Pd or Pt.

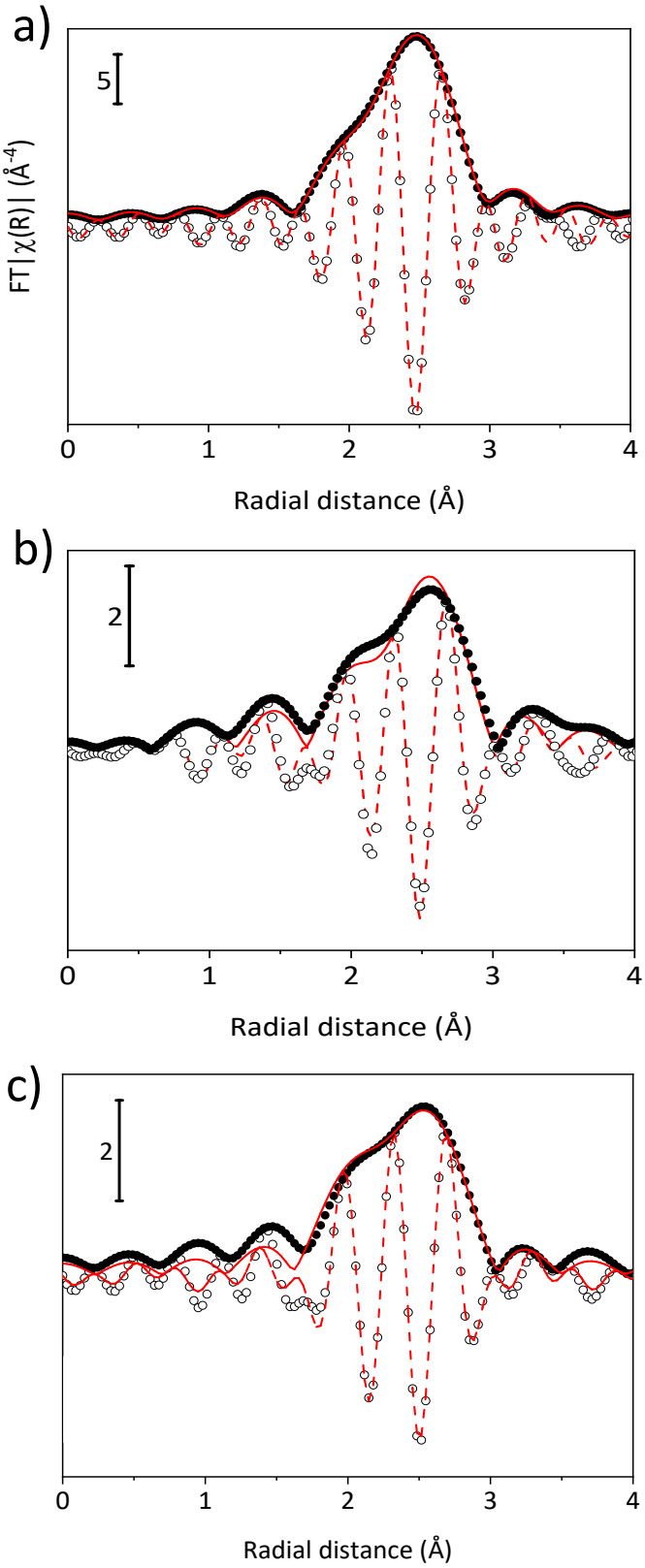

Figure S8: Phase-uncorrected Fourier-Transform of the k^3-weighted EXAFS function for XAS spectra recorded at the Pd K-edge for a) a Pd metallic foil, and b) a monometallic 0.5Pd/MgO catalyst, and c) a bimetallic 1.0PdPt/MgO catalyst, both synthesized via oxidative metal redispersion at 1073 K, followed by *in situ* reduction at 773 K under flow 20%H_2/N_2. Scatter traces correspond to experimental data (full dots: moduli, open dots: imaginary part), and lines to the fits (full line: moduli, dashed line: imaginary part).

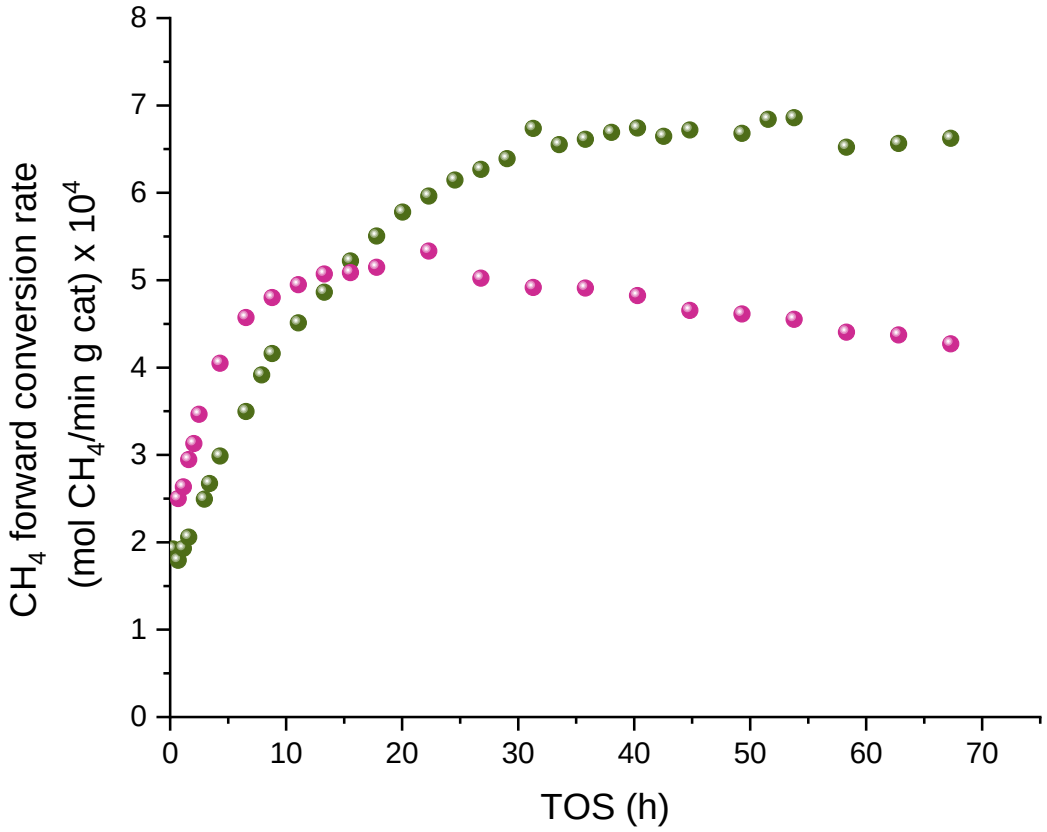

Figure S9: Evolution of the CH_4 forward conversion rate with the time-on-stream for 1.0PdPt/MgO catalysts activated from the same dry impregnate precursors via ether air-calcination at 623 K (pink symbols) or the same followed by air-annealing at 1073 K (oxidative metal redispersion into single-atom species, green symbols), followed by reduction in 20%H_2/Ar at 673 K. Reaction conditions: T=923 K, P= 1 bar, gas feed Ar/CH_4/CO_2 = 4.4/1.5/1.0 (molar), WHSV= 6.9 h^{-1}.

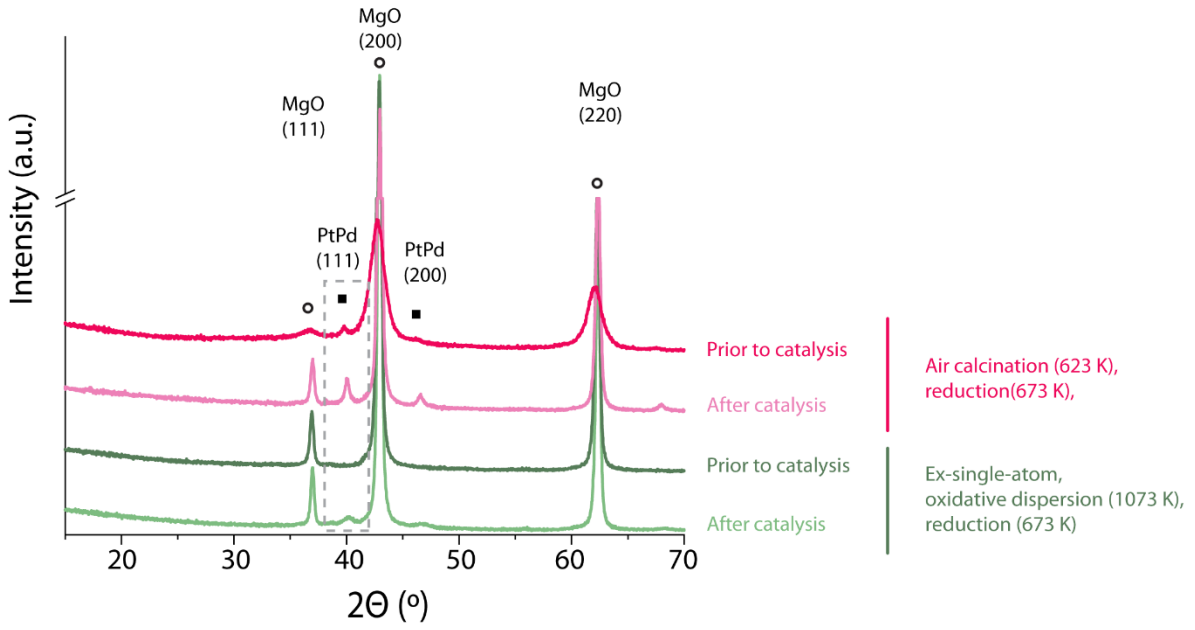

Figure S10: X-ray diffractograms for 1.0PdPt/MgO catalysts synthesized via either air calcination (623 K) or the same followed by oxidative redispersion (1073 K), followed by reduction in 20%H_2/N_2 (673 K), prior to catalysis (i.e. as-reduced) and after 70 hours on-stream in the dry reforming of methane with carbon monoxide (923 K). The dashed box highlights the (111) diffraction ascribed to PdPt alloys.

Following reduction activation, metal species are XRD-silent for the catalyst synthesized via oxidative redispersion, as a result of the very small size of the bimetallic PdPt nanoclusters developed from the single-atom precursor. Following prolonged exposure to catalysis conditions, a very weak and broad diffraction signal ascribable to PdPt alloys is observed, indicating that metal crystal growth is very limited during catalysis, resulting in only very small crystalline domains. The reference catalyst synthesized via conventional air calcination shows weak albeit comparatively sharper diffractions for PdPt alloys after reduction, associated to the larger metal crystals obtained on the MgO surface (Figures 2 and 7 in the main text). After exposure to catalysis, metal diffractions became notably more intense and sharper, indicating a significant growth of metal crystals during exposure to reaction conditions.

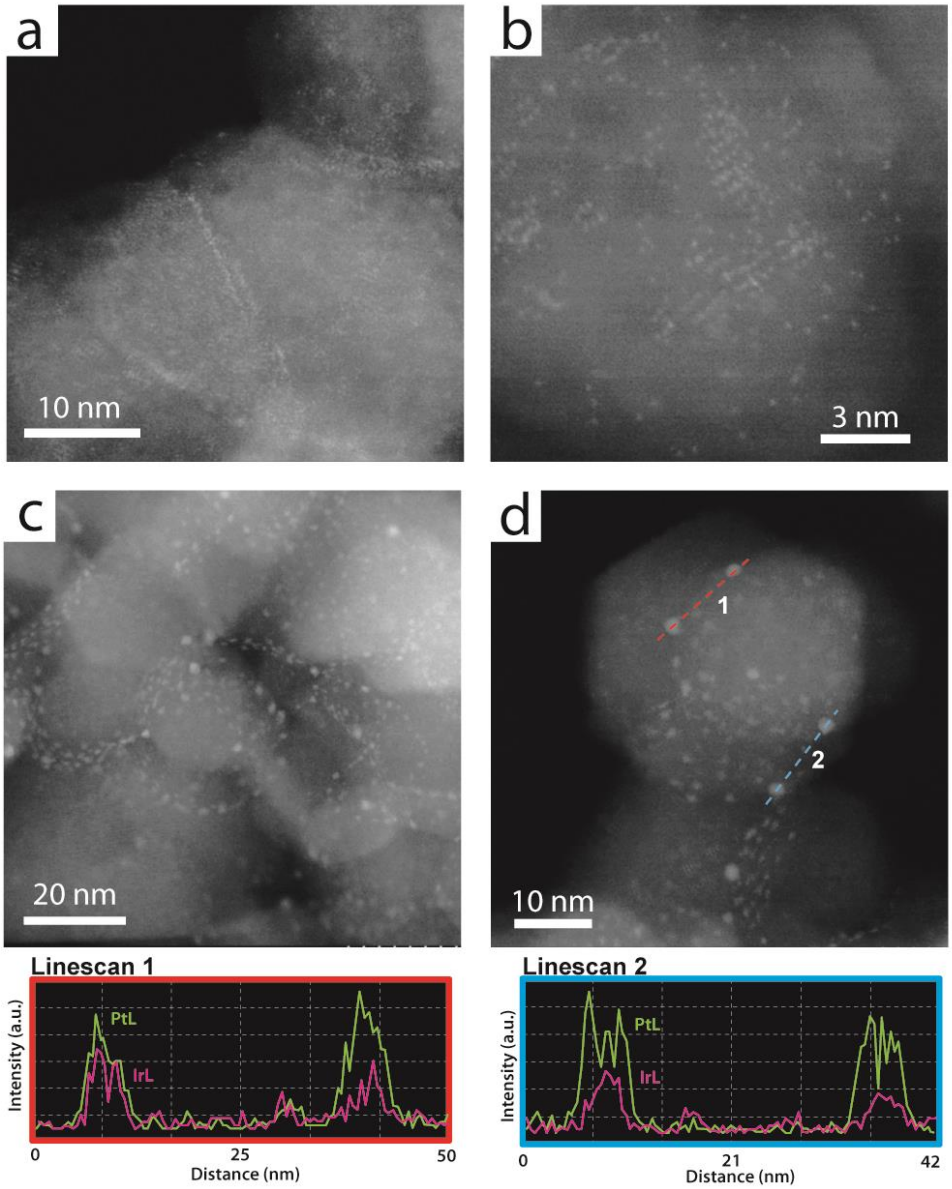

Figure S11: Representative HAADF-STEM micrographs of a IrPt/MgO catalyst (Ir:Pt=1) obtained by decomposition of the metal precursors in air, followed by oxidative metal redispersion in air at 1073 K (a,b), and following subsequent H_2-reduction at 773 K (c-d). Bottom panels show the compositional EDS results, based on PtL and IrL spectral signals for the linescans indicated on panel (d).

2. Supplementary Tables

Table S1. Nominal metal loading for the series of PdPt/MgO bimetallic materials.

Sample	Atomic ratio	Metal loading			
	Pd:Pt (at:at)	δ[a] (M_{at} nm^{-2})	Pd (wt%)	Pt (wt%)	(Pd+Pt) (wt%)
0.2PdPt/MgO	1:1	0.2	0.1	0.2	0.3
0.5 PdPt/MgO	1:1	0.5	0.2	0.5	0.6
1.0 PdPt/MgO	1:1	1.0	0.4	1.0	1.4
2.0 PdPt/MgO	1:1	2.0	0.7	2.0	2.7
4.0 PdPt/MgO	1:1	4.0	1.2	4.2	5.4

[a]Overall (Pd+Pt), based on the specific surface area determined after air-annealing at 1073 K.

Table S2. Summary of free parameters derived from the EXAFS fitting using DFT-optimized model structures for Pd stabilized in MgO. See Figures 4 and S6 for the corresponding spectra and models. Spectra fitting has been performed according with an approach previously described in Sarma et al. *J. Am. Chem. Soc.*, 2020, 142, 14890–14902.

Model	S_0^2	E_0 (eV)	σ^2 Pd-O ($Å^2$)	σ^2 Pd-O-Mg ($Å^2$)	R Pd-O (Å)	R Pd-O-Mg (Å)	r-factor
Pd atom under MgO step-edge (Figure 4)	0.8 ± 0.1	-5.8 ±2.0	0.0020 ±0.0016	0.0013 ±0.0031	2.199 ± 0.068	2.965 ± 0.022	0.031
Pd at regular sub-surface position (Figure S6)	0.6 ±0.1	-4.5 ±1.2	0.0020 ±0.0011	0.0097 ±0.0018	2.0153 ±0.0020	2.987 ±0.0097	0.016

S_0^2: amplitude reduction factor, E_0: energy shift, σ^2: Debye-Waller factor, R: radial distance, r-factor: goodness of fit. For fitting, the *k* and R ranges considered were 3-12 $Å^{-1}$ and 1-3.1 Å, respectively. The r-factor goodness-of-fit is the weighted mean value of the Pd-O and Pd-O-Mg scattering paths.

Table S3. Summary of free parameters derived from the EXAFS fitting using DFT-optimized model structures for Pt stabilized in MgO. See Figures 4 and S6 for the corresponding spectra and models. Spectra fitting has been performed according with an approach previously described in Sarma et al. *J. Am. Chem. Soc.*, 2020, 142, 14890–14902.

Model	S_0^2	E_0 (eV)	σ^2 Pt-O ($Å^2$)	σ^2 Pt-O-Mg ($Å^2$)	R Pt-O (Å)	R Pt-O-Mg (Å)	r-factor
Pt atom under MgO step-edge (Figure 4)	1.0 ± 0.2	6.9 ± 1.9	0.0019 ±0.0025	0.0030 ±0.0027	2.256 ±0.053	3.00 ±0.002	0.066
Pt at regular sub-surface position (Figure S6)	0.7 ± 0.1	7.7 ± 1.7	0.0016 ±0.0024	0.0038 ±0.0027	2.026 ±0.020	3.00 ±0.002	0.061

S_0^2: amplitude reduction factor, E_0: energy shift, Δr: variation in bond length with respect to model, σ^2: Debye-Waller factor, R: radial distance, r-factor: goodness of fit. For fitting, the *k* and R ranges considered were 3-12 $Å^{-1}$ and 1-3.1 Å, respectively. The r-factor goodness-of-fit is the weighted mean value of the Pt-O and Pt-O-Mg scattering paths.

Table S4. Summary of free parameters derived from the fitting of the PdK-EXAFS spectra for the bimetallic 1.0PdPt/MgO catalyst after *in situ* reduction at 773 K under flow of 20%H_2/N_2. For comparison, the fitting results for the corresponding monometallic 0.5Pd/MgO and a Pd metallic foil are also included.

Sample	Scattering path	CN	σ^2 ($Å^2$)	R (Å)	E_0 (eV)	r-factor
Pd foil	Pd-Pd	12[a]	0.0050 ±0.0005	2.7436 ±0.003	-4.4 ±0.6	0.00026
0.5 Pd	Pd-Pd	3.7[a] ±1.4	0.0085 ±0.0031	2.7806 ±0.02	-0.3 ±405	0.00337
0.5 (Pt+Pd)	Pd-Pd Pd-Pt	2.5[a] ±0.8 2.1[a] ±0.9	0.005 ±0.003	2.7513 ±0.0274	3.5 ±3.2	0.00087

[a] S_0^2=0.77±0.05 as derived from the fit for the Pd foil. For fitting, the *k* and R ranges considered were *k*=4-10.8 $Å^{-1}$; R=1.8-3 Å. CN: coordination number, σ^2: Debye-Waller factor, R: radial distance, E_0: energy shift, r-factor: goodness-of-fit.